IEEE Access
Multidisciplinary | Rapid Review | Open Access Journal

Received October 23, 2018, accepted November 9, 2018, date of publication November 16, 2018,
date of current version December 18, 2018.

Digital Object Identifier 10.1109/ACCESS.2018.2881732

Analysis and Design of a Wideband Coaxial Transition to Metal and Printed Ridge Gap Waveguide

ISLAM AFIFI, (Graduate Student Member, IEEE), MOHAMED MAMDOUH M. ALI, (Student Member, IEEE), AND ABDEL-RAZIK SEBAK, (Life Fellow, IEEE)
Electrical and Computer Engineering Department, Concordia University, Montreal, QC H4B 1R6, Canada
Corresponding author: Islam Afifi (i_afifi@encs.concordia.ca)

ABSTRACT In this paper, a wideband coaxial to ridge gap transition is proposed and implemented. The transition has a compact size, wide bandwidth, and simple structure. It can be used to excite ridge gap waveguides implemented by the printed circuit board or computer numerical control (CNC) technologies. A similar circuit model for a coax-to-microstrip junction is proposed and used to establish a systematic design procedure for the proposed transition. Perfect electric conductor and perfect magnetic conductor (PMC) boundaries are used to make the procedure independent of the fabrication technology. The PMC is replaced by a bed of nails for ridge gap realized by CNC technology and mushroom-shaped structure in the case of PCB technology. The proposed transition based on the PCB technology is fabricated and measured. There is a good agreement between simulated and measured results which validates the proposed design. The transition has a 59.22% bandwidth with $S_{11} < -10$ dB and $S_{21} > -0.5$ dB.

INDEX TERMS Ridge gap, coaxial transition, millimeter wave, wideband.

I. INTRODUCTION

Millimeter wave (mmw) band has gained great attention in the past several years for its wide unlicensed bandwidth, which makes it a good candidate in imaging and wireless communication systems. For imaging applications, mmw frequency band is preferred over the conventional X-ray imaging, because of its non-ionized radiation feature that makes it safe for human health. Also, its abilities to penetrate common clothes and reflect from the human body and metal objects enable it to be a suitable candidate for imaging security applications such as concealed weapon detection [1]–[3]. Furthermore, the wide bandwidth facilitates going through different field depth to construct 3D security image [4]. Regarding communication systems, high data rates and the ability to accommodate a huge number of connected devices with low latency and reliable connection are required. Hence, mmw band is a good candidate to achieve high data rates and serve high speed applications as more spectrum is available [5].

These features of mmw motivate the research community to exert more effort in providing microwave components with the state of the art guiding structure technologies working at this frequency band. One of the promising guiding structures is the ridge gap waveguide (RGW), which was introduced for the first time in 2009 [6]–[8] as a quasi-TEM guiding structure. This guiding structure is introduced in many forms such as metal and printed RGW [9]. The metal RGW can be realized by CNC technology, whereas the printed RGW is implemented using a traditional PCB technology. It is a promising guiding structure for mmw systems as the propagating mode is a quasi-TEM inside an air gap providing low signal distortion and low losses compared to microstrip line and substrate integrated waveguide (SIW) [10] technologies. Different electromagnetic devices are implemented using this technology such as filters, directional couplers, and antennas [11]–[19]. Hence, high performance transitions are required to excite these components. The common technique to excite the ridge gap structure is accomplished by inserting a microstrip line in the air gap of the RGW structure. It is widely used to excite both metal and printed RGW [20]–[25]. The major disadvantage of this feeding technique is the use of an end launch connector which has high insertion loss. Another way to excite the RGW is through the use of a coaxial transition. It is introduced in many configurations such as half wavelength open circuit [8] and quarter wavelength short

circuit [26]. These techniques exhibit a narrow bandwidth performance and sensitivity for probe position. Broadband transition designs are introduced in [26] and [27] by deploying a multi-sections matching transformer and fitting parts connected to the RGW. Although this technique has a wide bandwidth performance, it has a large size resulting in a bulky structure connected to the microwave devices. Beside that, it is limited to metal RGW structures due to the use of different heights in the transition. On the other hand, relatively few trials have been done to excite the printed RGW using a coaxial transition but they show a narrow bandwidth performance [13], [14]. The use of a waveguide to ridge gap transition is introduced in [28]–[30] for metal RGW and in [9] for the printed type. It is a narrow band for printed type and can achieve wideband for the metal type but it makes the device bulky.

This work is about designing a wide bandwidth coaxial to RGW transition based on a systematic design procedure. The proposed design is validated for both metal and printed RGW in different frequency bands. It has achieved a wide bandwidth performance with a compact size. This feature enables its integration with other microwave components and reduces the overall cost while covering the possible operating bandwidth of RGW (usually an octave frequency range).

This paper is organized as follows: Section II presents the design procedure of the transition. Section III shows the implementation of the transition to excite metal RGW structures in two different frequency bands. In Section IV, the implementation of the proposed transition in printed RGW is presented. The prototype, measured results, and performance analysis of the proposed transition in the printed RGW technology are presented in Section V. Finally, a summary of the paper outcomes is in Section VI.

II. COAXIAL TO RIDGE TRANSITION DESIGN PROCEDURE

The proposed transition from a coaxial line to RGW structure is designed in three stages: (1) introducing a circuit model for the direct connection between the coaxial and the RGW using ideal model with PEC and PMC boundaries (This makes the design procedure easier and independent of the implementation technology) (Section II-A), (2) employing a matching technique to increase the operating bandwidth (where the initial values of the proposed transition parameters are calculated) (Section II-B), and (3) replacing the PMC boundary by bandgap unit cells designed to cover the operating frequency band and an optimization process is performed to achieve better matching level (Section III and IV).

A. MODELING OF DIRECT TRANSITION FROM COAXIAL TO RGW

The design of the proposed transition starts by examining the direct connection between a coaxial line and the RGW shown in Fig. 1 (a). The width of the ridge (W=1.75 mm) and the air gap height (h=0.289 mm) are chosen to achieve a 50 Ω characteristics impedance to be matched with a standard 50 Ω coaxial line. This connection can be modeled by a π-circuit as

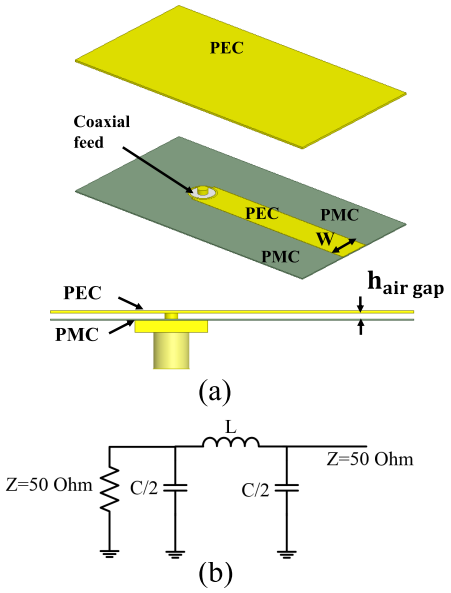

FIGURE 1. (a) Coaxial to ridge gap transition in HFSS using perfect magnetic conductor boundary condition. (b) The π-circuit model of the direct connection between the coaxial and the RGW.

shown in Fig. 1 (b) [31], where there are two capacitors (C/2) and one inductor (L), the inner conductor of the coaxial line acts as an inductor and the outer radius of the coaxial line with the top ground acts as a capacitor. The advantage of using a direct connection between a coaxial line and the RGW over the usage of a quarter or a half wavelength stub [8], [26] is the elimination of a frequency dependent section to achieve a wideband performance.

In order to extract the π-circuit parameters, the direct connection between the coaxial and the RGW is simulated in high frequency structure simulator (HFSS) with perfect boundary conditions. The reflection coefficient, obtained from HFSS simulation, is used to calculate the input impedance as follows:

$$Z_{insimulation} = Z_0 \frac{1 + S_{11}}{1 - S_{11}} \tag{1}$$

The input impedance for the circuit model can be expressed as

$$\begin{aligned} Z_{in\ model} &= \left(Z_0 \| \left(\frac{1}{j\omega C/2} \right) + j\omega L \right) \| \left(\frac{1}{j\omega C/2} \right) \\ &= \frac{Z_0(1 - \frac{\omega^2 LC}{2}) + j\omega L}{(1 - \frac{\omega^2 LC}{2})(1 + j\frac{\omega C Z_0}{2}) + j\frac{\omega C Z_0}{2}} \end{aligned} \tag{2}$$

By equating the input impedance of (1) with the input impedance of the circuit model (2), the values of the capacitance (C) and inductance (L) of the π-circuit model shown in Fig. 1 (b) can be obtained. As there are two equations (one for the real part and the other for the imaginary part) and two variables, the equations are consistent and there is only one solution.

Fig. 2 shows the obtained capacitance and inductance of the circuit model. It can be seen that they are stable in the

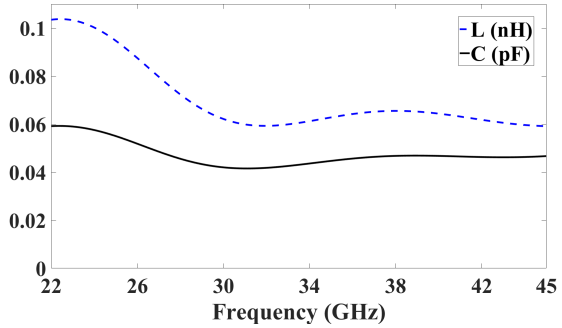

FIGURE 2. The capacitance and inductance of the π-circuit model obtained using the S-parameters from the HFSS simulation.

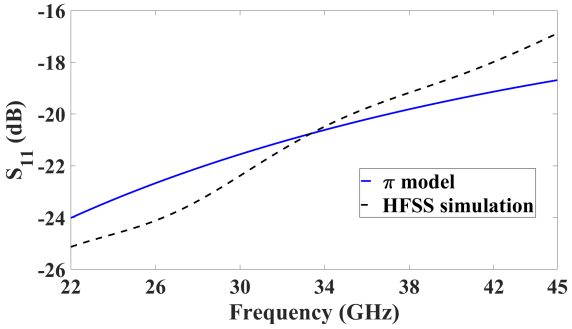

FIGURE 3. Comparison between the S- parameter obtained from the π model with that obtained from HFSS simulation.

region from 30 to 45 GHz. By choosing the values at the center frequency (33.5 GHz), the obtained capacitance and inductance are C=0.043 pF, and L=0.0605 nH, respectively. Fig. 3 shows the agreement between the reflection coefficient obtained from the π-circuit model and that from the simulator.

In order to improve the impedance matching even further, the input impedance of the direct connection is investigated. The real and imaginary parts of the input impedance are shown in Fig. 4. Since the reactance part is capacitive, an inductive element is required to have a pure real impedance that can be easily matched with the 50 Ω coaxial line. In addition, since the value of the real part of the impedance is declining with the frequency, an inductance and a tapered matching section are added to have a matched transition with 50 Ω ridge line impedance, making the proposed transition compatible with most of the microwave components.

The circuit model with the added parallel inductor (L_2) is shown in Fig. 5. Note that the tapering section is not considered here for simplicity of the circuit model. The new input impedance, after adding (L_2) becomes:

$$Z_{in\ total} = j\omega L_2 \| \frac{Z_0(1-\frac{\omega^2 LC}{2})+j\omega L}{(1-\frac{\omega^2 LC}{2})(1+j\frac{\omega CZ_0}{2})+j\frac{\omega CZ_0}{2}} \tag{3}$$

Here, the value of L_2 is optimized to minimize the reflection coefficient which can be expressed as:

$$\Gamma = \frac{Z_{in\ totoal} - 50}{Z_{in\ total} + 50} \tag{4}$$

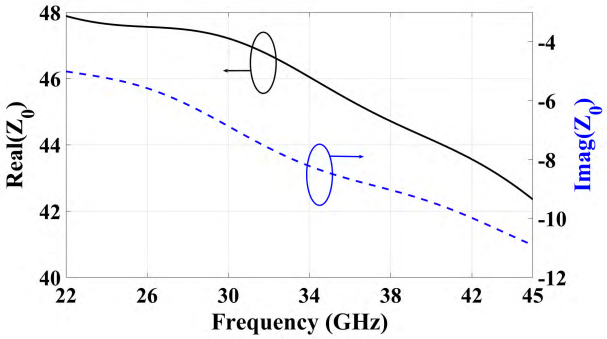

FIGURE 4. Real and imaginary part of the input impedance of the direct connection between coaxial and the ridge.

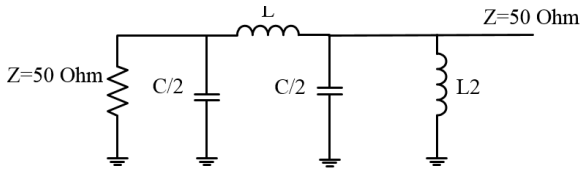

FIGURE 5. The circuit model of the direct connection with the added parallel inductor (L_2).

The conventional way to add a parallel inductance to a transmission line is through adding a shorted stub with a certain length. This technique produces an inductance that is changing with frequency and will limit the bandwidth of the proposed transition. In the proposed work, vias around the line are used to act as inductors to avoid such limitation. The value of the inductance depends on the radius and the height of the vias. Since the height is fixed in this work, the radius of the vias is the parameter that can be used in the optimization. Another parameter is the position of the vias with respect to the ridge line, as the field is decaying away from the ridge line (see Fig. 15 for the printed ridge gap case). These two parameters are used in the optimization process to have good matching.

B. PROPOSED TRANSITION STRUCTURE

A high matching level transition is required to excite the RGW. By using a single connection with perfect boundary conditions, the matching level in the direct connection approach −17 dB in the frequency band from 22 to 45 GHz. For a back-to-back configuration, the matching level will degrade further. Moreover, by replacing the PMC with the bandgap unit cells, the matching level becomes even worse. In this section, $S_{11} < -20$ dB over the whole frequency band is achieved in the ideal case. Therefore, when realizing the transition, it reaches the acceptable range of about −15 dB.

Fig.6 shows the total proposed transition in which a matching section and vias are used. Fig. 7 depicts S_{11} result from HFSS along with that of the direct connection with/without parallel inductance, where $L_2 = 1.3$ nH is the optimum value for good matching level. It is clear that the matching bandwidth ($S_{11} < -20$ dB) is wider and the matching level

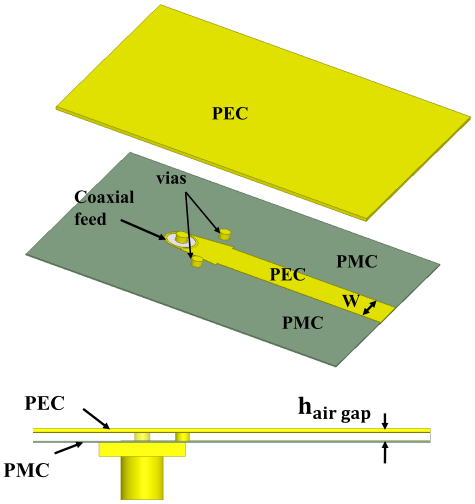

FIGURE 6. The geometry of the proposed transition with a tapered matching section and vias around the line.

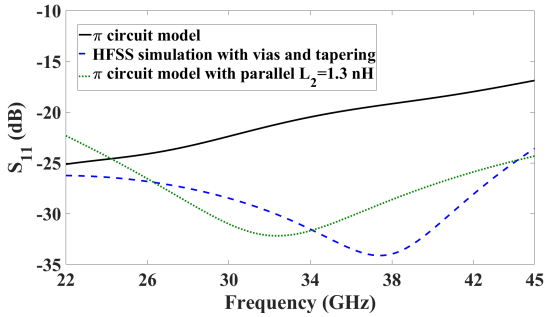

FIGURE 7. Comparison between the reflection coefficients of the π-circuit model, the π-circuit model with the added parallel inductor, and the simulated transition with the tapering and vias.

is improved especially at higher frequencies. As the principle of operation has been elaborated in the ideal case with PEC and PMC boundaries, the implementation of this transition in metal RGW and printed RGW is presented in the following sections.

III. METAL RIDGE GAP TRANSITION

The design of the proposed transition in metal RGW is presented in two frequency bands. For the frequency band from 12 to 22 GHz, the structure of the unit cell which is used to realize the artificial magnetic conductor (AMC) and the associated band gap for a single unit cell are shown in Fig. 8 and those for the unit cell with the added ridge line are shown in Fig. 9, where β is the propagation constant and a is the period of the unit cell. The band gap of the unit cell alone is from 9.11 to 25.03 GHz, while it becomes from 9.93 to 25.05 GHz when the ridge line is included. The propagating mode (QTEM) appears because of the added ridge line between the unit cells and propagates along the line. The appearance of extra modes, in the dispersion diagram of the unit cells with the ridge line, is due to the truncation of the periodic boundary in the direction normal to the

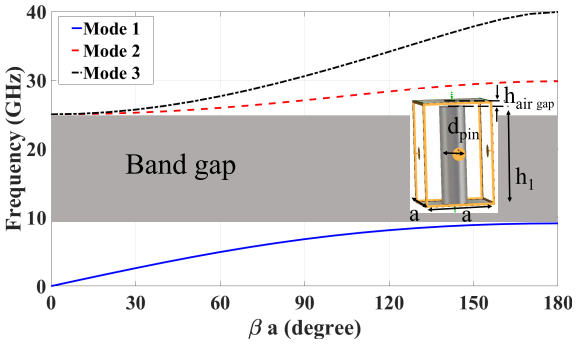

FIGURE 8. Dispersion diagram of a single unit cell for the Ku band.

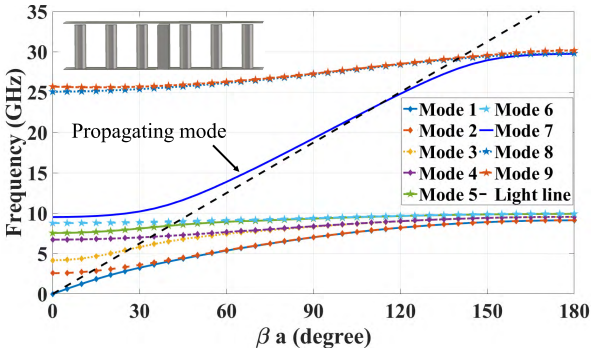

FIGURE 9. Dispersion diagram of the unit cell with the ridge line for the Ku band.

line [8]. While in the single unit cell case, the periodicity is on two directions, normal to the line and along the line, which assumes infinite structure and only one TM mode can propagate below the band gap and higher order TM and TE modes can propagate after the band gap.

The geometry of the back-to-back configuration of the proposed transition is illustrated in Fig. 10. The design of the ridge gap waveguide with 50 Ω characteristic impedance is done by using the stripline model [8] to calculate the initial width of the ridge line W_{line}. Then adjustment has been done using the computer simulation technology (CST) simulator, at the center frequency, to obtain the line width for matching with a 50 Ω coaxial line. A tapered section and four pins around the ridge line are then used to have an acceptable matching level. Finally, an optimization for the tapered section and the four vias is done to compensate for the capacitance and inductance introduced by the unit cells near the transition. The final dimensions are presented in Table 1. Fig. 11 shows the simulated S-parameters for the back-to-back configuration of the proposed transition. The impedance matching bandwidth ($S_{11} < -10$ dB) is from 12 to 22 GHz which covers the whole Ku band (from 12-18 GHz). Furthermore, the S_{21} is above -0.5 dB over the whole frequency band and S_{11} is less than -15 dB in most of the band.

Applying the same concept to a different frequency band, mainly from 24 to 40 GHz, is presented to validate our

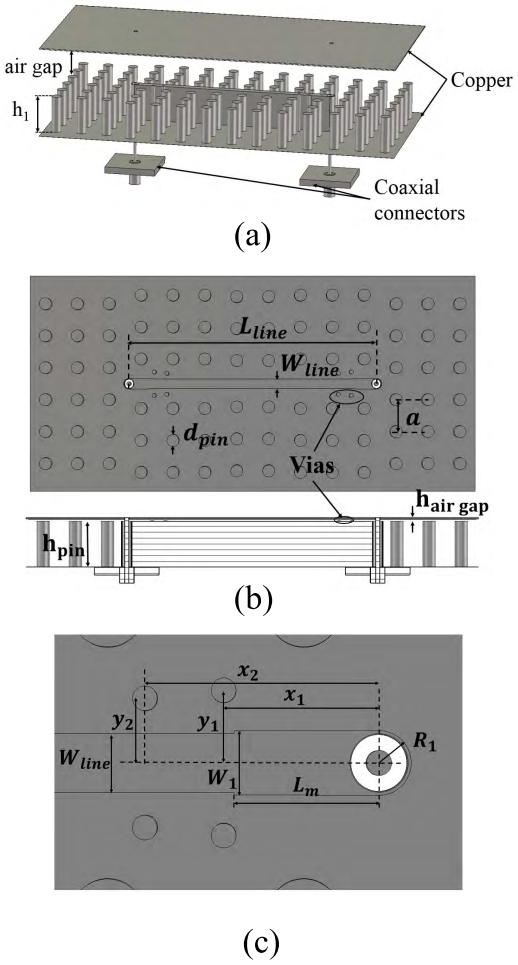

FIGURE 10. The geometry of the coaxial to metal ridge gap transition in the frequency range from 12 to 22 GHz. (a) The whole structure. (b) The top and side view (upper layer removed to show the structure). (c) The transition section. *(some inner unit cells are removed to make the geometry compact.)*

TABLE 1. The dimensions of the coaxial transition for metal ridge gap in the frequency range 12-22 GHz.

Dimension		Value in (mm)
Coaxial outer raduis (R_1)		0.668
Matching length (L_m)		2.949
Matching width(W_1)		1.297
Ridge width(W_{line})		1.2
Unit cell period (a)		4
Pin diameter (d_{pin})		1.5
Pin height (h_{pin})		5.6
Gap height (h_{airgap})		0.289
Total line length (L_{line})		55.06
Via 1	x_1	3.161
	y_1	1.471
Via 2	x_2	4.765
	y_2	1.309

design concept. For this frequency band, there is a need for a different unit cell to behave like AMC. The band gap of the new unit cell is from 20.05 to 45.65 GHz for the single unit cell, and from 21.6 to 44.6 GHz for the unit cell with

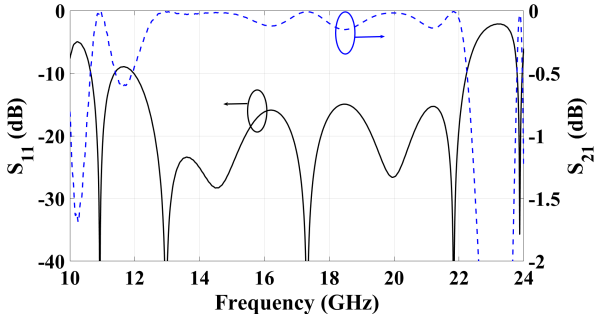

FIGURE 11. S-parameters of the coaxial to metal ridge transition in the frequency range from 12 to 22 GHz.

TABLE 2. The dimensions of the coaxial transition for metal ridge gap in the frequency range 24-40 GHz.

Dimension		Value in (mm)
Coaxial outer raduis (R_1)		0.644
Matching length (L_m)		3.289
Matching width(W_1)		1.506
Ridge width(W_{line})		1.2
Unit cell period (a)		2
Pin diameter (d_{pin})		1.0
Pin height (h_{pin})		2.8
Gap height (h_{airgap})		0.289
Total line length (L_{line})		26.8
Via 1	x_1	1.547
	y_1	1.347
Via 2	x_2	2.396
	y_2	1.433

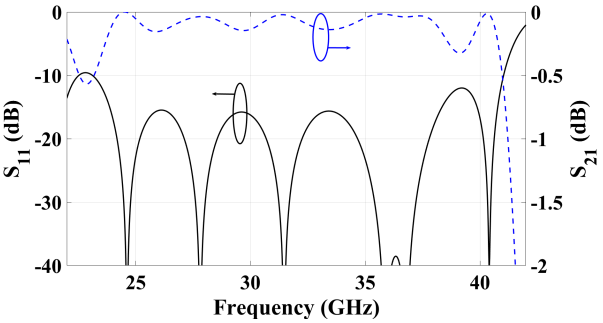

FIGURE 12. S-parameters of the coaxial to metal ridge transition in the frequency range from 24 to 40 GHz.

the ridge line. The dimensions of the unit cell and the back-to-back configuration of the transition are in Table 2. Fig. 12 shows the simulated S-parameters. The impedance matching bandwidth ($S_{11} < -10$ dB) is from 23.18 to 41 GHz and the S_{21} is better than -0.5 dB. The transition covers the whole Ka band (27-40 GHz), which makes it suitable for 5G communication and imaging applications.

IV. PRINTED RIDGE GAP TRANSITION

In this section, the proposed transition is applied to the printed ridge gap. Only one frequency band is presented here to avoid the redundancy. The selected frequency band is 24-40 GHz. The mushroom-shaped unit cell is used for the printed RGW.

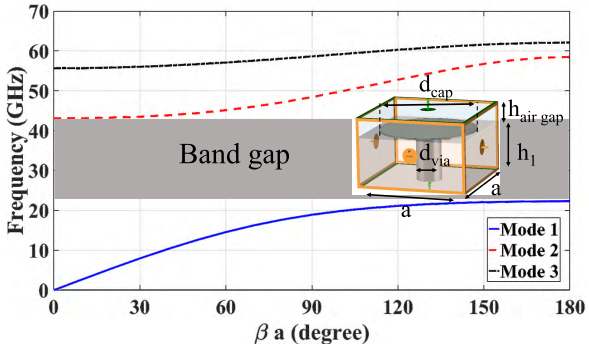

FIGURE 13. Dispersion diagram of a single unit cell for the Ka band in the printed ridge gap technology.

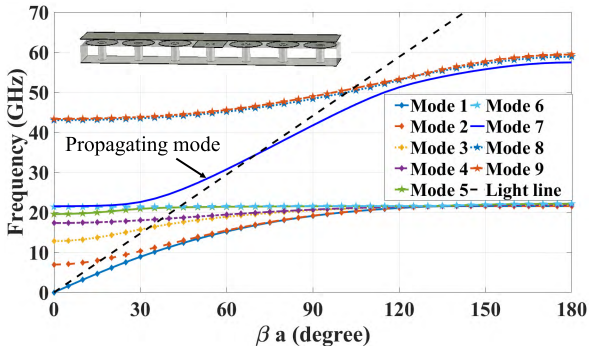

FIGURE 14. Dispersion diagram of the unit cell with the ridge line for the Ka band in the printed ridge gap technology.

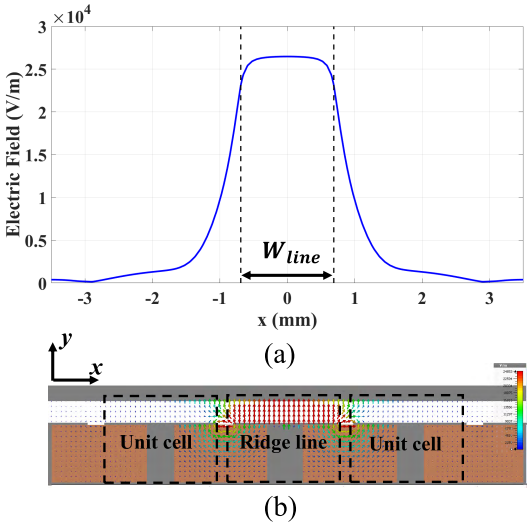

FIGURE 15. (a) The magnitude of the electric field in the middle of the air gap region. (b) Electric field distribution on the printed RGW at 30 GHz.

The unit cell with its band gap is illustrated in Fig. 13, where the used substrate material is Roger RT6002 (ε_r=2.94 and $tan\delta$=0.0012). The band gap is from 22.307 to 43.095 GHz for the single unit cell, and from 22.15 to 43.014 GHz for the unit cell with the ridge line as illustrated in Fig. 14. Another RT6002 substrate with 0.254 mm thickness is used

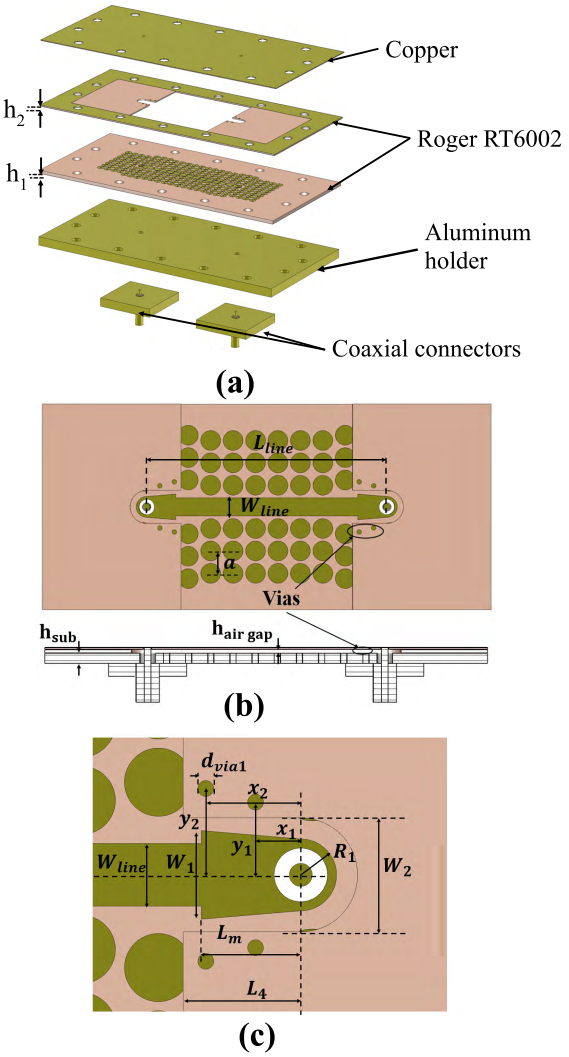

FIGURE 16. The geometry of the coaxial to printed ridge gap transition in the frequency range from 24 to 40 GHz. (a) The whole structure. (b) The top and side view (upper layer removed to show the structure). (c) The transition section. *(some inner unit cells are removed to make the geometry compact.)*

as a middle substrate while the center is removed to introduce the air gap. The vias around the transition are inserted in this substrate. The electric field distribution on the RGW cross section is shown in Fig. 15. The result shows that the use of the band gap unit cells around the ridge line has confined the electric field within the ridge line section.

Fig. 16 shows the configuration of the proposed transition. Fig. 17 shows the electric field distribution in the middle of the air gap region and along the transition. The final dimensions are shown in Table 3. The S-parameters are shown in Fig. 19 along with the measurement results, where the impedance matching bandwidth ($S_{11} < -10$ dB) is from 22.7 to 41.8 GHz and the S_{21} is greater than -0.5 dB. Once again, the transition covers the whole Ka band (27-40 GHz). This transition is fabricated to validate the concept of the proposed technique.

TABLE 3. The dimensions of the coaxial transition for the printed ridge gap technology in the frequency range 24-40 GHz.

Dimension		Value in (mm)
Coaxial outer raduis (R_1)		0.79
Matching length (L_m)		2.2
Matching width(W_1)		1.95
Ridge width(W_{line})		1.38
Unit cell period (a)		1.7
unit cell via diameter (d_{via})		0.39
unit cell cap diameter (d_{cap})		1.5
Pin height (h_{pin})		2.8
Gap height (h_{airgap})		0.289
Middle substrate inset length (L_4)		2.6
Middle substrate inset width (W_2)		2.508
Matching via diameter (d_{via1})		0.35
Total line length (L_{line})		52.2
Via 1	x_1	1
	y_1	1.6
Via 2	x_2	1.1
	y_2	1.9

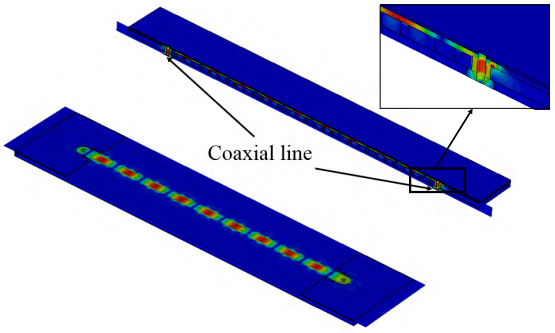

FIGURE 17. Electric field distribution of the coaxial to printed RGW transition.

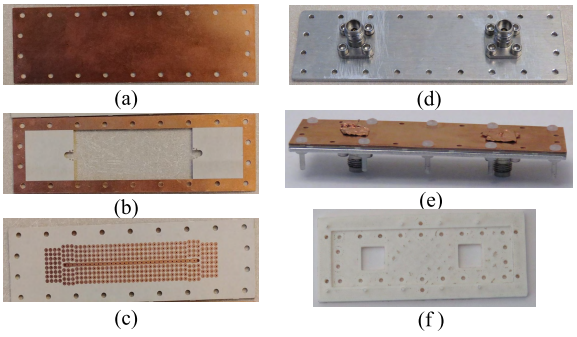

FIGURE 18. The fabricated prototype of the proposed transition in the printed ridge gap technology. (a) Top layer. (b) Middle layer. (c) Bottom layer. (d) Aluminum holder. (e) Assembled structure. (f) Plastic holder.

V. MEASUREMENT AND DISCUSSION

The fabricated parts of the proposed transition using conventional PCB technology together with the integrated prototype are shown in Fig. 18. For measurement purposes, an aluminum base has been drilled with the same PCB drilling machine and the plastic housing has been fabricated using 3D printing. A conducting copper tab has been used on top of the structure instead of soldering to connect the inner pin of the coaxial line to the upper copper plate. The (N52271A)

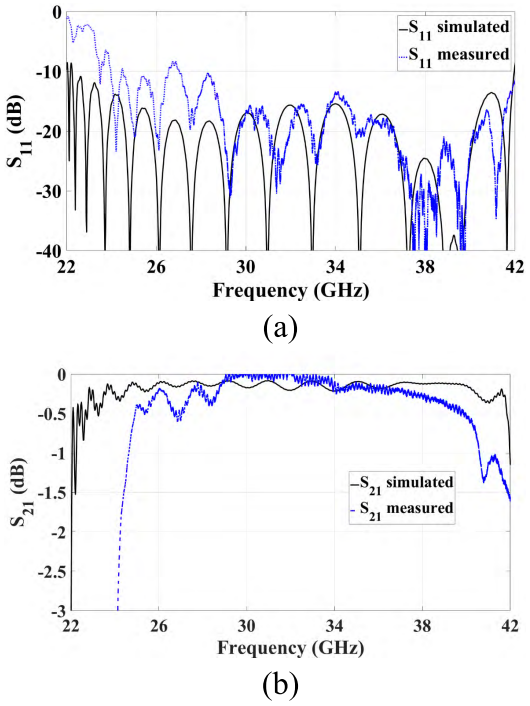

FIGURE 19. Comparison between simulated and measured S-parameters for the proposed transition. (a) S_{11} and (b) S_{21}.

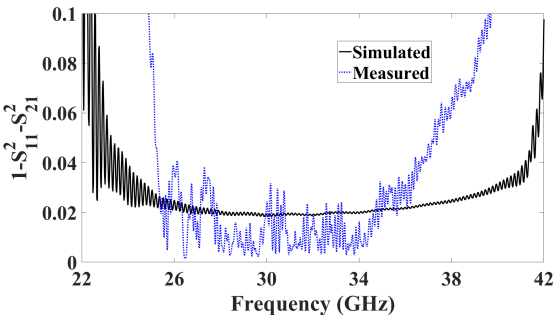

FIGURE 20. Power loss factor ($1 - S_{11}^2 - S_{21}^2$).

PNA network analyzer, the Electronic calibration kit (Ecal), and 2.4 mm coaxial connectors are used through the measurement. There is a good agreement in the behavior between the measured and simulated results as shown in Fig. 19. The proposed transition achieves -10 dB matching level over the whole frequency band (24-40 GHz) with insertion loss less than 0.5 dB. The discrepancy in the amplitudes at the start of the band, between measured and simulated results, is due to the misalignment between the layers, the tolerance in the fabrication, and the contact between the connector and the ground of the ridge gap substrate. The measured performance is a fractional bandwidth of 45.8% (from 24.9-39.7 GHz) with $S_{11} < -8.3$ dB and $S_{21} > -0.5$ dB. The power loss factor $(1 - S_{11}^2 - S_{21}^2)$ [32] is shown in Fig.20, for simulated and measured results. The simulated power loss factor is less than 0.04 over the operating band and mean value of the measured

TABLE 4. Comparison between various types of transition in the metal and printed ridge gap technologies.

	Technology	Feeding type	Fractional bandwidth (%)	Return loss (dB)	Insertion loss (dB)	Length
[30]	metal	WR62	58% (12-19 GHz)	10	-	5.5 mm (0.284 λ_0)
[21]	metal	microstrip	46.05% (11.7-18.7 GHz)	10	0.3	15.7 mm (0.796 λ_0)
[23]	metal	microstrip	20.87% (55.8-68.8 GHz)	20	0.5	-
[8]	metal	coaxial	26.67% (13-17 GHz)	8	1	10 mm (0.5 λ_0)
[26]	metal	coaxial	85.71% (10-25 GHz)	15	0.15	46.68 mm (2.723 λ_0)
[27]	metal	coaxial	96.63% (11.5-33 GHz)	15	1	58 mm (4.3 λ)
[9]	Printed	WR15	17.89% (56-67 GHz)	10	1.5	Direct connection
[20]	Printed	microstrip	38.6% (23-34 GHz)	15	0.5	-
[22]	Printed	microstrip	55.17% (21-37 GHz)	10	1	-
[24]	Printed	microstrip	37.04% (27.5-40 GHz)	10	0.8	-
[14]	Printed	coaxial	28.19% (10.97-14.57 GHz)	15	0.35	Direct connection
This work	Printed	coaxial	59.22% (22.7-41.8 GHz)	10	0.5	2.6 mm (0.28 λ_0)

one is in a good agreement with the simulated one. The increase of the insertion loss and hence the power loss factor at the beginning and the ending of the operating frequency band may come from dielectric and copper losses. The fields must be exponential decaying away from the ridge line (in the band gap region of the unit cell surrounding the ridge line) and as the operating frequency reaches the edges of the band gap region the exponential decaying is weak and hence the fields suffer from the dielectric and copper losses. The reason of high losses in the measurement rather than in the simulation may come from the fact that the simulation uses the dielectric loss tangent at 10 GHz but the measurement takes the real value at the millimeter wave frequency range (22-42 GHz) which is higher than the value at 10 GHz.

A performance comparison between the proposed design and other related work in the literature is presented in Table 4. The proposed transition performance is better than most of the reported transitions [8], [9], [14], [20]–[24], [30] in terms of the fractional bandwidth. Reported results in [26] and [27] show a better fractional bandwidth performance, but they are bulky (non-planar structures) and electrically large (length is more than 2.5 λ_0) compared to the proposed transition and only suitable for CNC technology. The proposed work is planar (which makes it suitable for both CNC and PCB technologies) and compact in size (0.28 λ_0) with reasonable return loss and insertion loss. The matching concept of the proposed transition is also scalable to different frequency bands as shown in section III. The use of the coaxial feeding avoids dielectric and radiation losses that exist in microstrip to ridge transitions [22], [24]. The proposed transition has superior performance over other small sizes (less than λ_0) coaxial to RGW transitions reported in [8] and [14]. It focuses on reducing the effect of the parasitic inductance and capacitance introduced by the direct connection between the coaxial line and the RGW and hence a wide bandwidth is achieved. The use of rectangular waveguide to excite the ridge gap is presented in [9] and [30], it can achieve a wideband matching but again makes the design bulky.

VI. CONCLUSION

In this paper, a wideband coaxial to ridge gap transition has been designed and implemented in metal and printed ridge gap technologies. A bandwidth of 59.22 % has been achieved for the printed type and 55.53 % for the metal type with insertion loss less than 0.5 dB. A circuit model for the coaxial to ridge gap transition is presented and it shows a good potential to be used in determining the required matching circuit parameters. The designed transition is planar, and henceforth, is applicable for both metal and printed RGW structures. The transition is compact in size and easy to fabricate which makes it suitable for small devices.

REFERENCES

[1] D. M. Sheen, D. L. McMakin, and T. E. Hall, "Three-dimensional millimeter-wave imaging for concealed weapon detection," *IEEE Trans. Microw. Theory Techn.*, vol. 49, no. 9, pp. 1581–1592, Sep. 2001.

[2] H. Zamani and M. Fakharzadeh, "1.5-D sparse array for millimeter-wave imaging based on compressive sensing techniques," *IEEE Trans. Antennas Propag.*, vol. 66, no. 4, pp. 2008–2015, Apr. 2018.

[3] Z. Briqech and A. R. Sebak, "Millimeter-wave imaging system using a 60 GHz dual-polarized AFTSA-SC probe," in *Proc. 33rd Nat. Radio Sci. Conf. (NRSC)*, Aswan, Egypt, Feb. 2016, pp. 325–332.

[4] D. M. Sheen *et al.*, "Wide-bandwidth, wide-beamwidth, high-resolution, millimeter-wave imaging for concealed weapon detection," *Proc. SPIE*, vol. 8715, p. 871509, May 2013.

[5] T. S. Rappaport, J. N. Murdock, and F. Gutierrez, Jr., "State of the art in 60-GHz integrated circuits and systems for wireless communications," *Proc. IEEE*, vol. 99, no. 8, pp. 1390–1436, Aug. 2011.

[6] A. U. Zaman, E. Rajo-Iglesias, E. Alfonso, and P.-S. Kildal, "Design of transition from coaxial line to ridge gap waveguide," in *Proc. IEEE Antennas Propag. Soc. Int. Symp.*, Charleston, SC, USA, Jun. 2009, pp. 1–4.
[7] P.-S. Kildal, "Three metamaterial-based gap waveguides between parallel metal plates for mm/submm waves," in *Proc. 3rd Eur. Conf. Antennas Propag.*, Berlin, Germany, Mar. 2009, pp. 28–32.
[8] P.-S. Kildal, A. U. Zaman, E. Rajo-Iglesias, E. Alfonso, and A. Valero-Nogueira, "Design and experimental verification of ridge gap waveguide in bed of nails for parallel-plate mode suppression," *IET Microw., Antennas Propag.*, vol. 5, no. 3, pp. 262–270, Mar. 2011.
[9] H. Raza, J. Yang, P.-S. Kildal, and E. A. Alós, "Microstrip-ridge gap waveguide–study of losses, bends, and transition to WR-15," *IEEE Trans. Microw. Theory Techn.*, vol. 62, no. 9, pp. 1943–1952, Sep. 2014.
[10] M. Bozzi, A. Georgiadis, and K. Wu, "Review of substrate-integrated waveguide circuits and antennas," *IET Microw. Antennas Propag.*, vol. 5, no. 8, pp. 909–920, Jun. 2011.
[11] M. M. M. Ali, S. I. Shams, and A. R. Sebak, "Printed ridge gap waveguide 3-dB coupler: Analysis and design procedure," *IEEE Access*, vol. 6, pp. 8501–8509, 2018.
[12] A. Farahbakhsh, D. Zarifi, and A. U. Zaman, "A mmWave wideband slot array antenna based on ridge gap waveguide with 30% bandwidth," in *IEEE Trans. Antennas Propag.*, vol. 66, no. 2, pp. 1008–1013, Feb. 2018.
[13] S. Birgermajer, N. Janković, V. Crnojević-Bengin, M. Bozzi, and V. Radonić, "Forward-wave 0 dB directional coupler based on microstrip-ridge gap waveguide technology," in *Proc. 13th Int. Conf. Adv. Technol., Syst. Services Telecommun. (TELSIKS)*, Oct. 2017, pp. 154–157.
[14] S. Birgermajer, N. Janković, V. Radonić, V. Crnojević-Bengin, and M. Bozzi, "Microstrip-ridge gap waveguide filter based on cavity resonators with mushroom inclusions," *IEEE Trans. Microw. Theory Techn.*, vol. 66, no. 1, pp. 136–146, Jan. 2018.
[15] M. M. M. Ali and A. r. Sebak, "Compact printed ridge gap waveguide crossover for future 5G wireless communication system," *IEEE Microw. Wireless Compon. Lett.*, vol. 28, no. 7, pp. 549–551, Jul. 2018.
[16] M. Farahani, M. Akbari, M. Nedil, T. A. Denidni, and A. R. Sebak, "A novel low-loss millimeter-wave 3-dB 90° ridge-gap coupler using large aperture progressive phase compensation," *IEEE Access*, vol. 5, pp. 9610–9618, 2017.
[17] A. Dadgarpour, M. S. Sorkherizi, and A. A. Kishk, "High-efficient circularly polarized magnetoelectric dipole antenna for 5G applications using dual-polarized split-ring resonator lens," *IEEE Trans. Antennas Propag.*, vol. 65, no. 8, pp. 4263–4267, Aug. 2017.
[18] S. I. Shams and A. A. Kishk, "Design of 3-dB hybrid coupler based on RGW technology," *IEEE Trans. Microw. Theory Techn.*, vol. 65, no. 10, pp. 3849–3855, Oct. 2017.
[19] M. S. Sorkherizi, A. Dadgarpour, and A. A. Kishk, "Planar high-efficiency antenna array using new printed ridge gap waveguide technology," *IEEE Trans. Antennas Propag.*, vol. 65, no. 7, pp. 3772–3776, Jul. 2017.
[20] M. S. Sorkherizi and A. A. Kishk, "Transition from microstrip to printed ridge gap waveguide for millimeter-wave application," in *Proc. IEEE Int. Symp. Antennas Propag. USNC/URSI Nat. Radio Sci. Meeting*, Vancouver, BC, Canada, Jul. 2015, pp. 1588–1589.
[21] B. Molaei and A. Khaleghi, "A novel wideband microstrip line to ridge gap waveguide transition using defected ground slot," *IEEE Microw. Wireless Compon. Lett.*, vol. 25, no. 2, pp. 91–93, Feb. 2015.
[22] M. S. Sorkherizi and A. A. Kishk, "Fully printed gap waveguide with facilitated design properties," *IEEE Microw. Wireless Compon. Lett.*, vol. 26, no. 9, pp. 657–659, Sep. 2016.
[23] U. Nandi, A. U. Zaman, A. Vosoogh, and J. Yang, "Millimeter wave contactless microstrip-gap waveguide transition suitable for integration of RF MMIC with gap waveguide array antenna," in *Proc. 11th Eur. Conf. Antennas Propag. (EUCAP)*, Paris, France, Mar. 2017, pp. 1682–1684.
[24] N. Bayat-Makou and A. A. Kishk, "Realistic air-filled TEM printed parallel-plate waveguide based on ridge gap waveguide," *IEEE Trans. Microw. Theory Techn.*, vol. 66, no. 5, pp. 2128–2140, May 2018.
[25] F. Fan, J. Yang, V. Vassilev, and A. Uz Zaman, "Bandwidth investigation on half-height pin in ridge gap waveguide," *IEEE Trans. Microw. Theory Techn.*, vol. 66, no. 1, pp. 100–108, Jan. 2018.
[26] S. I. Shams and A. A. Kishk, "Wideband coaxial to ridge gap waveguide transition," *IEEE Trans. Microw. Theory Techn.*, vol. 64, no. 12, pp. 4117–4125, Dec. 2016.
[27] M. A. Nasr and A. A. Kishk, "Wideband inline coaxial to ridge waveguide transition with tuning capability for ridge gap waveguide," *IEEE Trans. Microw. Theory Techn.*, vol. 66, no. 6, pp. 2757–2766, Jun. 2018.
[28] D. Zarifi, A. Farahbakhsh, A. U. Zaman, and P. S. Kildal, "Design and fabrication of a high-gain 60-GHz corrugated slot antenna array with ridge gap waveguide distribution layer," *IEEE Trans. Antennas Propag.*, vol. 64, no. 7, pp. 2905–2913, Jul. 2016.
[29] Z. Talepour and A. Khaleghi, "A K-band planar slot array antenna on a single layer ridge gap waveguide," in *Proc. 11th Eur. Conf. Antennas Propag. (EUCAP)*, Paris, France, Mar. 2017, pp. 1685–1689.
[30] F. Ahmadfard and S. A. Razavi, "Bandwidth and gain enhancement of ridge gap waveguide H-plane horn antennas using outer transitions," *IEEE Trans. Antennas Propag.*, vol. 66, no. 8, pp. 4315–4319, Aug. 2018.
[31] D. M. Pozar, *Microwave Engineering*, 4th ed. Hoboken, NJ, USA: Wiley, 2011.
[32] G. M. Rebeiz, *RF MEMS: Theory, Design, and Technology*. New York, NY, USA: Wiley, 2003.

ISLAM AFIFI (GS'18) received the B.Sc. degree in electronics and communication engineering and the M.Sc. degree in engineering physics from Cairo University, Cairo, Egypt, in 2009 and 2014, respectively. He is currently pursuing the Ph.D. degree in electrical and computer engineering with Concordia University, Montreal, QC, Canada. His research interests are millimeter-wave microwave components and antennas. He was a Teaching and Research Assistant with the Engineering Mathematics and Physics Department from 2009 to 2014, and a Senior Teaching Assistant from 2014 to 2016.

MOHAMED MAMDOUH M. ALI (S'15) received the B.Sc. (Hons.) and M.Sc. degrees in electronics and communications engineering from Assiut University, Egypt, in 2010 and 2013, respectively. He is currently pursuing the Ph.D. degree in electrical and computer engineering from Concordia University, Montreal, QC, Canada. From 2010 to 2015, he was a Teaching and Research Assistant with the Department of Electronics and Communications Engineering, Assiut University. He was a Teaching and Research Assistant with Concordia University. His current research interests include microwave reciprocal/nonreciprocal design and analysis and antenna design.

ABDEL-RAZIK SEBAK (LF'18) received the B.Sc. degree (Hons.) in electrical engineering from Cairo University, Cairo, Egypt, in 1976, the B.Sc. degree in applied mathematics from Ein Shams University, Cairo, in 1978, and the M.Eng. and Ph.D. degrees in electrical engineering from the University of Manitoba, Winnipeg, MB, Canada, in 1982 and 1984, respectively. From 1984 to 1986, he was with Canadian Marconi Company involving in the design of microstrip phased array antennas. From 1987 to 2002, he was a Professor with the Department of Electronics and Communication Engineering, University of Manitoba. He is currently a Professor with the Department of Electrical and Computer Engineering, Concordia University, Montreal, QC, Canada. His research interests include phased array antennas, millimeter-wave antennas and imaging, computational electromagnetics, and interaction of EM waves with engineered materials and bioelectromagnetics. He is a member of the Canadian National Committee of International Union of Radio Science Commission B. He was a recipient of the 2000 and 1992 University of Manitoba Merit Award for Outstanding Teaching and Research, the 1994 Rh Award for Outstanding Contributions to Scholarship and Research, and the 1996 Faculty of Engineering Superior. He has served as the Chair of the IEEE Canada Awards and Recognition Committee from 2002 to 2004, and as the Technical Program Chair of the 2002 IEEE CCECE Conference and the 2006 URSIANTEM Symposium. He is the Technical Program Co-Chair for the 2015 IEEE ICUWB Conference.